Experimental Study on Response Law and Failure Process of Slopes in Fully Weathered Granites Under Precipitation Infiltration

Fei Tan (tanfei@cug.edu.cn)
China University of Geosciences

Research Article

Keywords: Fully weathered granite, Precipitation infiltration, Precipitation -induced landslide, Matrix suction, Weber similarity criterion

Posted Date: March 10th, 2021

DOI: https://doi.org/10.21203/rs.3.rs-263219/v1

Abstract

To investigate the response law and failure process of slopes in fully weathered granites under precipitation infiltration, a typical fully weathered granite slope is selected for sampling in Fengkai, Guangdong. The physical simulation experimental study of rainfall-induced landslide is conducted, in which Weber criterion is used as the similarity criterion for precipitation. The research results reveal that under precipitation infiltration, the fully weathered granite slope responds quickly. Further, the water content increases sharply, and the matrix suction quickly dissipates. After dissipation, the matrix suction transforms into pore water pressure, which accelerates the deformation of the slope. The wet peak has a large infiltration depth in the slope, and the acceleration of deep part is lower than that of the shallow part. Under the action of precipitation, the fully weathered granite model undergoes four stages of failure. Firstly, gullies and cracks appear. Secondly, cracks propagate and link up. Then, the soil on the slope surface swells and ruptures. Finally, the slope slides locally until the entire slope creeps, collapses, and transforms into a "soil flow." Based on the analysis of precipitation similarity, the landslide will be triggered in fully weathered granite slope by precipitation when the precipitation intensity comes up to 155 mm/d, and the landslide occurs at an accumulated precipitation of 304 mm. Overall, the results can provide a reliable theoretical basis and abundant experimental data for the prevention, monitoring, and forecasting of geological disasters in granitic areas.

1. Introduction

Precipitation is one of the most important factors that can induce slope instability (Huang and Fan 2013; Segoni et al. 2018). The landslide caused by precipitation-induced slope instability is termed as precipitation-induced landslide (Segoni et al. 2018; Dai and Lee 2001), which accounts for 90% of the total landslides (Li et al. 2004). In particular, the weathered granite distribution area in South China is a landslide prone area with precipitation-induced, small and shallow landslide. This is because the climate in southern China is hot and rainy, the granite suffers strong erosion, denudation, and cutting. Consequently, the rock mass structure in the granite distribution area is loose, there is a thick weathering crust, and landslide often occurs (Pradhan and Kim 2014, 2015). Meanwhile, the vegetation coverage is high in South China, so landslides have the characteristics of strong concealment, sudden outbreaks, and they can induce great damage, which makes early warning and forecasting quite difficult.

Consequently, precipitation-induced landslides have garnered extensive research attention. Various physical models have been proposed to describe the slope instability induced by precipitation infiltration (Dietrich et al. 1995; Chen and Lee 2003; Li et al. 2011; Bai et al. 2014; Zêzere et al. 2015). Landslides in weathered granite crust have also attracted global research attention, mainly from two aspects: firstly, the stability of the granite slope has been examined through field and laboratory tests using sensitivity analysis and structural characterization of weathered rock and soil (Pradhan and Kim 2014, 2015; Liu et al. 2008); secondly, laboratory tests and numerical simulations have been employed to analyze the influence of precipitation infiltration, seepage field, and water content distribution on the stability of granite slope (Zheng et al. 2005). However, there are few studies on the change law of pore water pressure and matrix suction, as well as slope deformation and failure process by simulating the whole process of precipitation infiltration using different strength theories. Large-scale physical experiments are even rarer. Hence, based on large-scale physical model tests, it is of great significance to study response law and failure process of fully weathered granite slope under precipitation infiltration and to explore the deformation and failure mechanism of precipitation-induced landslide in fully weathered granite.

In this study, Fengkai, Guangdong in South China, which has a wide distribution of granite and exhibits a subtropical monsoon climate, is considered as a case study. The climate is warm throughout the year with sufficient sunlight, strong weathering of granite, rich precipitation, and an average annual precipitation of 1480.0 mm. Weathering provides the material basis, and precipitation induces landslide. The landslides in this area are relatively developed, especially in the flood season. Several precipitation-induced landslides and other geological disasters occur every year. Field surveys have revealed that the precipitation-induced landslides in the granite area of Fengkai are mainly shallow and small. For example, in Fengchuan, a total of 74 landslides have been catalogued. In particular, numerous landslides occur along the interface of full weathered and strong weathered zones, and the landslide body is in the state of "slide", "peeling", and "soil flow". Further, such a landslide exhibits multiple periods of sliding (see Fig. 1), demonstrating a repeated disaster process of "gradual weathering - precipitation-induced landslide - gradual weathering - precipitation re-induced landslide". Here, to examine the fully weathered granite slope as a case study, samples are taken from a typical fully weathered granite slope in the county and transported to the laboratory. Using a large-scale laboratory-based physical model test, the deformation response of fully weathered granite soil under the coupling of precipitation infiltration and hydraulics is analyzed.

2. Experimental

2.1 Similarity criterion for precipitation

The large-scale laboratory physical simulation tests should satisfy the size and precipitation similarity ratio requirements. According to the hydraulic model test, the Weber criterion can be used as the similarity criterion for modeling the precipitation of precipitation-induced fully weathered granite slope (Heller 2011; Liu et al. 2020). Weber criterion is a similarity criterion for water flow whose main force is surface tension (Liu et al. 2020). According to the similarity criterion, the scaling relation and size of corresponding rainfall duration, precipitation intensity, and precipitation can be obtained. This criterion can be expressed as follows (Heller 2011):

$$We = \frac{\rho v^2 l}{\sigma} \tag{1}$$

If the surface tension coefficient and current density of the prototype and the model are equal, the similarity ratio of precipitation intensity and the physical test model is

$$\lambda_v = \lambda_l^{-\frac{1}{2}} \tag{2}$$

The similarity ratio of rainfall duration and the physical model is

$$\lambda_t = \lambda_l^{\frac{3}{2}} \tag{3}$$

Hence, according to the precipitation intensity and rainfall duration, the similarity ratio precipitation and the physical model are equal, i.e.,

$$\lambda_Q = \lambda_v \times \lambda_t = \lambda_l \quad (4)$$

where σ is the surface tension coefficient of water, N/m; ρ is the current density, kg/m^3; v is the characteristic velocity, m/s; l is the characteristic length, m; λ_v is the similarity ratio of precipitation intensity; λ_t is the similarity ratio of rainfall duration; λ_l is the similarity ratio of physical model; λ_Q is the similarity ratio of precipitation.

According to the similarity principle, the similarity ratio of the model is selected based on the sizes of the slope prototype and model box. The similarity ratio of the basic physical parameter of soil is set to 1, the slope height of the model box is set to 2m, and the similarity ratios of other parameters are calculated by the model similarity ratio. Table 1 lists the similarity relation of the geometric and physical parameters between the experimental prototype and the model. Herein, the similarity ratios of precipitation intensity and precipitation are calculated according to Eqs. (2) and (4), respectively.

Table 1 Similarity ratio of fully weathered granite slope

	Scaling relation	Scale	Prototype	Model
Slope height (cm)	λ_l	8.5	1700	200
Precipitation intensity (mm/h)	$\lambda_{v=}\lambda_l^{-1/2}$	0.34	-	-
Precipitation (mm)	$\lambda_{Q=}\lambda_l$	8.5	-	-

2.2 Test parameters and layout

According to the test objective, it is necessary to ensure that the laboratory test slope has sufficient similarity with the original slope and that the precipitation can reproduce the slope instability. Thus, the shape and strength parameters of the laboratory slope are particularly important. In this experiment, the fully weathered granite soil in Fengkai is employed for modeling the slope (see Fig. 2), and the empirical parameters of remoulded soil are used for calculation. The calculation parameters are shown in Table 2. Based on the inversion calculation of the limit equilibrium state, the original slope state can be restored in the laboratory and the precipitation-induced landslide can be replicated.

Table 2 Physical and mechanical parameters of fully weathered granite soil

Natural unit weight (kN/m^3)	Saturated unit weight (kN/m^3)	Saturated undrained shear strength		Saturated drained shear strength		Permeability coefficient
		Internal friction angle (°)	Cohesion c (kPa)	Internal friction angle (°)	Cohesion c (kPa)	K_{20} (cm/s)
18.2	19.4	20	8	28	7	2.35×10^{-3}

The size of the model box is 6.0m×2.0m×2.8m., the incline of model slope is set to 60°. A schematic of the experimental setup including the displacement meter, tension meter, and water content sensor is shown in Figure 3. A total of four earth pressure sensors, named SP1, SP2, SP3, and SP4, are utilized to test the horizontal and

vertical earth pressure. Further, 19 displacement labels and 3 layers of horizontal white sand strips are arranged in the observation window to examine soil displacement and deformation.

2.3 Precipitation simulation

A precipitation valve and a flow meter were used to simulate precipitation. The water pipe, which was equipped with multiple water outlets, was installed at the top of the physical model. A sprinkler was set on the water outlet pipe, and nozzle hole was used to adjust the precipitation.

There is abundant precipitation in Fengkai, and the amount of precipitation in one day is usually large. Based on the local meteorological data, the interval between precipitation events was determined. The precipitation process of this model test is intermittent precipitation, and the slope slides induced after four precipitations are applied (see Table 3). The intensities of four precipitations are 10, 19, 12, and 11 mm/h, and the precipitation durations are 30, 30, 24, and 90 min, respectively. According to the precipitation interval of Fengkai, the interval of four precipitations is set to 35, 110, and 1406 min, and the prototype accumulated precipitation is 43, 123, 164, and 304 mm, respectively.

Table 3 Simulated precipitation scheme

Record number	Simulation parameters for the precipitation process				Precipitation scale	Prototype precipitation intensity (mm/d)	Prototype accumulated precipitation (mm)
	Test time	Duration (min)	Precipitation capacity (m^3)	Precipitation intensity (mm/h)			
1	11.22 11:15-11:45	30	0.0201	10	8.5	82	43
2	11.22 12:20-12:50	30	0.0391	19		155	123
3	11.22 14:40-15:04	24	0.0197	12		98	164
4	11.23 14:30-16:00	90	0.0682	11		90	304

3. Analysis Of Slope Response Under Precipitation Infiltration

3.1 Analysis of slope deformation

3.1.1 Horizontal deformation of slope

This is because the soil is cracked here, so the local soil of the slope flips rapidly under precipitation infiltration, which drives the slider to move into the slope. Subsequently, the displacement of L5 measurement point stabilizes until 27 min after the fourth precipitation occurs. Its deformation rate increases rapidly, and it continues to move into the slope. After the accumulated inward displacement exceeds 7 mm, landslide occurs. During the second

precipitation, the displacement of L7 measurement point initially increases and then slows down. After the second precipitation stops, the horizontal displacement of L7 measurement point increases sharply, and then the infiltration process lasts for nearly 2 h. During this period, the slope deformation rate is reduced, but the deformation does not stop. The curve for L1 measurement point is similar to that of L7 measurement point. After the second precipitation, the horizontal deformation rate of L1 measurement point quickly increases to 0.0952 mm/min. After 30 min, the deformation rate is reduced. After the third precipitation, its deformation rate again rises rapidly, reaching 0.2965 mm/min, and then the deformation rate reduces to 0.00078 mm/min until 12 min after the start of the fourth precipitation. The horizontal deformation rate at L1 measurement point rises to 0.1625 mm/min, the deformation increases to 17.6 mm, and the slope begins to lose stability. After the third precipitation initiates, the accumulated precipitation reaches 12.235 mm, the slope deformation rate rises sharply to 1.8357 mm/min at L7 measurement point, and the deformation increases from 3.8 mm to 15.97 mm in a very short period. After the precipitation stops, the displacement of L7 measurement point continues to rise, but the increase is slower, and the deformation stops after nearly 30 min. The slope deformation at L3 measurement point increases to 5.07 mm after 8 min of the third precipitation. A crack appears on the edge of the slope at this time, which drives the slider to flip. L3 measurement point moves into the slope, and the displacement is -0.4 mm. After the precipitation stops, the deformation slowly restores to its original condition and develops toward the free side of the slope. After the fourth precipitation, the displacement increases sharply to 3.66 mm, and landslide occurs. After the fourth precipitation begins, the slope deformation accelerates again, and the horizontal deformation rate at L1 measurement point increases to 0.1625 mm/min. The horizontal displacement rate at L7 measurement point rises to 0.1391 mm/min. After nearly 1 h, L1 and L7 measurement points slide. Throughout the experiment, L9 and L11 measurement points remain located at the edge and outside of the precipitation range, so they are almost undamaged.

3.1.2 Vertical deformation of slope

The vertical deformation of each measurement point is presented in Figure 5. After the first precipitation, the deformations at L2, L4, L6, L8, L10, and L12 measurement points are not obvious, indicating that the slope is relatively stable in the vertical direction. L2 measurement point begins to rapidly deform 15 min after the second precipitation starts. Then, L4 measurement point begins to deform, and the overall trend is that the deformation rate increases during precipitation, and it decreases after the precipitation. The measurement point L8 exhibits a slow vertical deformation after the second precipitation at a rate of nearly 0.0009 mm/min, and no vertical deformation occurs at L6, L10, and L12 measurement points. After the third precipitation, the deformation at L6 measurement point increases slowly initially and then rapidly, and the maximum displacement reaches 7.8 mm. The displacement of L2, L4, and L8 measurement points rise rapidly, reaching a rate of 1.52 mm/min. Moreover, the vertical displacement of L8 measurement point increases sharply, and after nearly 25 min, the cracks at the slope surface coalescence. Approximately 30 min after the precipitation, the maximum displacement reaches 20.4 mm, and the maximum width of the slope surface crack is nearly 8 cm. During the third precipitation period, L10 and L12 measurement points that are less affected by the precipitation exhibit almost no vertical deformation. After the fourth precipitation begins, slope deformation accelerates again. Except for L10 and L12 measurement points, the vertical deformation rates of L2, L4, L6, and L8 measurement points rise sharply. The vertical displacement rate of L8 measurement point reaches 1.6512 mm/min, and the maximum displacement is 39.42 mm. The vertical displacements of L2, L4, and L6 measurement points are 11.2, 2.3, and 9.9 mm, respectively, and landslide occurs.

Overall, the horizontal and vertical deformations of slope under precipitation occur at different speeds and locations. The response rate of horizontal deformation is higher than that of vertical deformation. Horizontal deformation first appears in the upper middle part of the slope, while vertical deformation first appears in the middle and lower part of the slope. Hence, weathered granite crust is initially deformed in the middle and upper part of the slope and then in the middle and lower part of the slope. This is an early sign of the landslide deformation of weathered granite crust and may be utilized for geological hazard assessment. Meanwhile, as the number of precipitation events and the accumulated precipitation increase, the slope deformation displacement rises. Horizontal and vertical deformations start with the first and second precipitations, respectively. After the third precipitation, both horizontal and vertical deformations occur obviously, and a large displacement deformation is observed until the fourth precipitation, where slope deformation accelerates again, and finally landslide occurs. It is clear that under the condition of previous accumulated precipitation, rapid and large deformation occurs in both horizontal and vertical directions, accelerating the failure and instability of the slope.

3.2 Analysis of matrix suction change

The matrix suction response of the slope is shown in Figure 6. The pore water pressure can be obtained from the observation point using a tensioner. When the pore pressure is negative, its absolute value represents the matrix suction. Ten minutes after the first precipitation, the matrix suction of the #2 measurement point located in the middle of slope drops rapidly to -32.5kPa, and it basically stabilizes at -2.2kPa. The #3 measurement point at the top of the slope is closest to the sprinkler, and its matrix suction rapidly declines from -77.8 to -2.0kPa and then tends to be nearly stable. The matrix suction of #1 measurement point changes gradually, while that of the #4 and #6 measurement points located in the deep part exhibit negligible variation. The matrix suction of #5 measurement points in the deepest part exhibits an increase instead of decrease, which may be attributed to the decrease in porosity of the slope due to the increase in its weight caused by precipitation. At the beginning of second precipitation, the matrix suction at #1 measurement point varies from -74.1kPa to a stable value of -3.0kPa in nearly 95 min. After the end of second precipitation, the matrix suction of #4 measurement point decreases to -0.1 kPa. However, the matrix suction of #5 measurement point keeps on increasing, and that of #6 measurement point also increases slowly. After the third precipitation, the matrix suction at #1-#4 measurement points is basically stable with a slight fluctuation, indicating a variation in the water content inside the soil and looseness of the soil. Further, 380 min after the end of third precipitation, the matrix suction at #5 and #6 measurement points tend to decrease, and the matrix suction of #6 measurement point 20cm away from the slope surface declines much faster than that of #5 measurement point 25cm away from the slope surface. After the fourth precipitation starts, the matrix suctions of #2 and #4 measurement points decrease to 0. The matrix suction of #4 measurement point continues to drop, and it becomes equal to the pore water pressure of 2.0kPa. The matrix suction of #6 measurement point declines linearly until -25.0kPa, where it stabilizes. The matrix suction of #1 and #3 measurement points continues to decrease, and landslide occurs when it drops to nearly -1.2kPa. As the #5 measurement point has the largest buried depth, the variation trend of matrix suction is gentle, which indicates that rainwater does not infiltrate to the depth of the #5 measurement point before landslide occurs.

Overall, the analysis indicates that as the number of precipitation events and the precipitation intensity increase, the matrix suction initially reduces rapidly and then slowly decreases until it transforms into pore water pressure, which accelerates the deformation of slope and the formation of landslide. Hence, the dissipation of matrix suction in unsaturated soil is the intrinsic reason for the occurrence of precipitation-type landslides.

3.3 Analysis of variation in water content

The water content response curve of the slope is shown in Figure 7. The intensity of the first precipitation is small. After the precipitation starts, the water content of each measurement point does not change. When the precipitation stops for 12 min, the water content of #2 measurement point closest to the slope surface increases first. After the second precipitation begins, the water content of #1 measurement point starts to increase, and the change in water content of the #2 and #4 measurement points lags behind that of 1#. After 12 min, the water content of #1, #2, and #4 measurement points increases sharply from 14.8% to 34.5%, from 14.29% to 29.6%, and from 16.9% to 29.3%, respectively. The water content of #3 measurement point changes a little later, and it significantly rises from 13.7% to 27.0% after the completion of the two precipitations. According to the analysis, it is inferred that due to the cracks in the middle of the slope at this time, precipitation infiltration causes the water content of #1, #2, and #4 measurement points to increase sharply, and the cracks do not propagate to the #3 measurement point yet. Though the distance to the slope is relatively low, rainwater does not infiltrate into the sensor position. During the stop of precipitation, the water content of #1 and #2 measurement points decreases significantly, and that of #4 measurement point declines slightly, which is directly related to the infiltration of rainwater into the cracks. After the third precipitation starts, the water content of #1, #2, and #4 measurement points no longer decreases but increases until the end of the precipitation. The water content of these measurement points increases to 37.4%, 30.0%, and 32.8%, respectively. After the precipitation stops, the water content of #1, #2, #3, and #4 measurement points gradually decreases, eventually reaching 27.9%, 23.4%, 22.6%, and 29.2% respectively. The intensity of the fourth precipitation is small, and it has a long duration. After 11 min of the start of the precipitation, the water content of #1, #2, #3, and #4 measurement points increases almost simultaneously, indicating that the position 10 cm away from the slope surface reaches a stable infiltration. After the fourth precipitation, the water content of #1, #2, #3, and #4 measurement points continues to increase, and finally landslide occurs. During the entire precipitation process, since the #5 and #6 measurement points are buried deeply, the water content remains basically unchanged. The fluctuation of the data in the figure is ascribed to the contact between the sensor and the soil.

Overall, this analysis reveals that water content of slope changes rapidly during the initial stage, and that of shallow soil increases sharply. After the third precipitation, the response curve tends to be flat, and the soil is basically saturated. The infiltration depth is limited, and the water content of the deeper measurement points remains basically unchanged.

3.4 Analysis of variation in the earth pressure

The response curve of earth pressure under precipitation infiltration is shown in Figure 8. Under precipitation infiltration, the earth pressure of SP1 and SP2 measurement points are changed. After the first and second precipitations, the horizontal earth pressure of SP1 measurement point increases from 8.602 kPa to 8.635 kPa and 9.166 kPa; after the third precipitation, it drops to 8.687 kPa, but there is almost no change after the fourth precipitation, and it remains stable at nearly 8.5 kPa. The vertical earth pressure of SP2 measurement point changes slowly during the early stage, and it increases to 26.162 kPa after the start of the second precipitation. As the precipitation continues to infiltrate, the vertical earth pressure continues to increase. After the fourth precipitation, the slope deforms significantly, and the vertical earth pressure of the SP2 measurement point continues to decrease until the slope becomes unstable.

Similarly, the earth pressure of SP3 and SP4 measurement points also change due to precipitation infiltration. After the first precipitation, the horizontal earth pressure of SP3 measurement point gradually varies from 7.3 kPa to 7.1 kPa. After the third precipitation, the horizontal earth pressure continues to decrease to 6.8 kPa. Meanwhile, the shallow soil of the slope exhibits an obvious deformation, and the slope is cracked. Due to the displacement and loosening of the soil, the horizontal earth pressure drops to 3.8 kPa. At this time, although the precipitation stops, the slope is still cracking. The horizontal earth pressure continues to decrease to 0.1 kPa. After the fourth precipitation begins, the slope severely deforms, and the earth pressure of SP3 measurement point is in free condition, which is almost reduced to 0 kPa, and then landslide occurs. The vertical earth pressure of SP4 measurement point changes slowly in the early stage. After the first three precipitations are completed, the weight of slope rises due to the precipitation, and the vertical earth pressure increases from 12.9 to 14.0 kPa. The rainwater continues to infiltrate. Further, the sensor and soil continue to be compressed, and the vertical earth pressure continues to increase to 14.8 kPa and then basically stabilizes until it is maximized (15.7 kPa) before the fourth precipitation. Then, the slope is significantly deformed, causing the soil to swell until the slope collapses.

Overall, the comprehensive analysis of the earth pressure response suggests that the slope weight increases due to precipitation infiltration, and the vertical earth pressure of SP2 and SP4 measurement points slowly increases. The SP1 measurement point located in the deep part of the slope is negligibly affected, and its earth pressure remains almost unchanged. The earth pressure of SP3 measurement point located in the deep part of slope decreases gradually at first. After the third precipitation, the horizontal earth pressure continues to decrease due to the displacement and loosening of the soil until it reduces to almost 0 kPa, and then landslide occurs.

3.5 Analysis of wetting peak change

The wetting peak response curve is shown in Figure 9. The wetting peak changes in three characteristic sections. The slope of the curve is maximum in the first and second precipitation stages, and the wetting peak moves fastest in the shallow soil. Even after the precipitation ends, the wetting peak continues to move deeper. After reaching a depth of 20 cm, the slope of this section becomes smaller, and the advancing speed of the wetting peak is significantly slower. After the third precipitation, the slope of this section continues to decrease. Here, the advancing speed of the wetting peak decreases again, and the advancing depth reaches 31 cm. After the fourth precipitation begins, the slope of this section becomes slightly steeper, and the infiltration depth continues to increase slowly until the depth exceeds 33 cm, and then the slope becomes unstable.

Under precipitation infiltration, the water content increases sharply and reaches a maximum of 37.4%. The deep measurement point is slightly affected, and its water content remains basically unchanged, indicating that water does not infiltrate 40 cm before the landslide occurs. The matrix suction quickly dissipates. The shallow matrix suction rapidly decreases to 0 kPa, and after it dissipates, it transforms into pore water pressure, which accelerates the deformation of the slope. The wetting peak gradually moves to the deep part, but the acceleration of the deep part is significantly less than the acceleration of the shallow part.

Overall, this analysis indicates that under precipitation infiltration, the slope response of fully weathered granite is rapid, and the wetting peak gradually moves to the deep part, but the acceleration of the deep part is less than that of the shallow part. This process also represents the gradual transformation of unsaturated soil to saturated soil.

3.6 Analysis of slope failure

Based on the physical simulation of precipitation infiltration of fully weathered granite slope, the slope failure can be divided into four stages (see Fig. 10). In the first stage, the slope surface layer is loose due to strong soil weathering, and precipitation can easily form small gullies (Figure 10-a). Under continuous precipitation, the slope surface produces small cracks, which slowly propagate. In the second stage, under precipitation infiltration, the water content of the soil increases continuously, the soil gradually enters the half-saturated state from the unsaturated state, the matrix suction decreases, and the effective stress and shear strength are reduced, and the interior part of the slope begins to enter an unstable state, and diagonal cracks appear to extend to the opposite side (Figure 10-b). In the third stage, under the continuous action of precipitation, the water content continues to increase, the shallow soil on the slope surface transforms from half-saturated state to saturated state, and the small cracks continue to expand into large cracks. The surrounding soil softens to form a bulge, and bulge rupture (Figure 10-c) also occurs locally. Since the shear strength of the soil continues to decrease, when the anti-sliding force of the local soil is less than the sliding force, the local block slide body ruptures. In the fourth stage, when the wetting peak of the slope is immersed to a certain depth, the shallow soil on the slope is almost saturated, and many bulges are formed on the slope. Due to gravity, the soil on the slope appear to slide. The failure process of fully weathered granite slope is different from that of classic rock slope. Under continuous precipitation infiltration, the entire slope does not slide instantly but creeps slowly toward the foot of the slope in the form of a "soil flow", and the slide body accumulates in a "tongue form" (Figure 10-d). Under the continued action of precipitation, the flowing water once again transforms the form of landslide soil accumulation, which eventually becomes a debris flow "accumulation fan".

According to the comprehensive analysis, the slope failure of fully weathered granite is quite different from the slope failure caused by the extension of the tension cracks on the top of classic weathering crust. This is ascribed to the special granite rock and soil. The fully weathered granite soil is relatively uniform in weathering, and the difference in the properties of the slope soil is small. Under precipitation, as the interior part of the soil gradually becomes saturated, cracks appear first in the upper and middle part of the slope. The soil around the cracks softens, and the shear strength becomes almost zero. The crack concentration area first shows flaky slide, and then expands to the entire slope surface. The slope gradually moves downward under the action of gravity, which causes the lower slide body to move faster than the upper slide body, and finally the entire slope is slowly collapsed.

4. Discussion

The precipitation process considered in the present model is an intermittent long-term strong precipitation. Under the action of four precipitation infiltrations, the slope becomes unstable. The intensity of the first precipitation is 10 mm/h (prototype precipitation intensity: 82 mm/d), which lasts for 30 min, and the accumulated precipitation after the end of precipitation is 4.25 mm (prototype precipitation: 43 mm). The intensity of the second precipitation is 19 mm/h (prototype precipitation intensity: 155 mm /d), which lasts for 30 min, and the accumulated precipitation is 12.325 mm (prototype precipitation: 123 mm) after the end of precipitation. The intensity of the third precipitation is 12 mm/h (prototype precipitation intensity: 98 mm/d), which lasts for 24 min, and the accumulated precipitation is 16.405 mm (prototype precipitation: 164 mm) after the end of precipitation. The intensity of the fourth precipitation is 11 mm/h (prototype precipitation intensity: 90 mm/d), which lasts for 90 min, and the accumulated precipitation 30.43 mm (prototype precipitation: 304 mm) after the end of precipitation.

Due to precipitation infiltration, the slope deformation, water content, matrix suction, and earth pressure change significantly. The response shows a certain lag relative to precipitation, and the variation in the parameters is highly correlated with precipitation. A precipitation intensity of 19 mm/h (prototype precipitation intensity: 155 mm/d) directly causes rapid crack expansion of the slope edge of the model, which continues to infiltrate the diagonal cracks, and then the middle slope collapses and deforms. When the accumulated precipitation reaches 30.43 mm (prototype precipitation: 304 mm), the slope slides with a maximum sliding depth of 13 cm and an average thickness of approximately 5 cm. Further, the front part of the accumulation area is nearly 23 cm away from the foot of the slope.

The proposed accumulated precipitation of landslides is based on precipitation similarity. The corresponding prototype precipitation threshold can be used as reference for the forecast of precipitation landslides in the test area. Further, in this study, Weber criterion is considered in the landslide model for the first time according to theoretical analysis. The criterion describes the similarity of precipitation infiltration, which needs to be experimentally confirmed. Meanwhile, the slope of the model is prepared in the laboratory, where the original structure of weathered soil is broken. Thus, the slopes of physical model and prototype are different. However, the results can reveal the internal mechanism of precipitation-induced landslides.

5. Conclusions

In this study, Weber criterion was used as the similarity criterion for precipitation to describe the slope stability of precipitation-induced fully weathered granite. The deformation response of fully weathered granite slope under the precipitation infiltration was examined, and the mechanics characteristics of slope instability, failure evolution, and destruction process were investigated. The main results of the study are summarized as follows:

(1) Under precipitation infiltration, the response of fully weathered granite slope response was rapid, which also represented the gradual transformation of unsaturated soil to saturated soil. Due to precipitation infiltration, the response rate of horizontal deformation was greater than that of vertical deformation. Horizontal deformation first appeared in the upper part of the slope, while vertical deformation first appeared in the middle and lower parts of the slope. Under the conditions of the previous accumulated precipitation, both horizontal and vertical directions exhibited a rapid and large deformation, which accelerated the slope failure and instability. The water content of shallow soil increased sharply, whereas the water content of deep part remained basically unchanged. The matrix suction quickly dissipated, and the shallow matrix suction reduced to zero in a short period. The wet peak gradually moved to the deep part, but the acceleration of the deep part was less than that of the shallow part, and the earth pressure continued to increase until slope failure.

(2) The slope failure of fully weathered granite occurred in four stages: appearance of gully, crack → crack expansion and infiltration → slope swelling, rupture → sliding and collapse of slope body, revealing a "soil flow" shape. These four stages were accompanied by precipitation infiltration. As the water content of soil increased, earth pressure also increased, which enhanced the sliding force, and the softening of precipitation reduced the shear strength of the rock and soil as well as the stability of the slope. The softening strength was revealed as a crucial factor for precipitation-induced landslide.

(3) The precipitation process and slope deformation failure showed obvious characteristic stages. Under precipitation infiltration, the pores of the soil were gradually filled with water, the soil lost its ability to absorb water, and the matrix suction was significantly reduced, i.e., the effective cohesion between soil particles was

significantly reduced. Then, the matrix suction dissipated and transformed into pore water pressure. This accelerated the deformation of the slope body and the formation of landslide. Hence, the dissipation of the matrix suction of unsaturated soil body was proved to be the inherent reason for the occurrence of precipitation-induced landslide.

(4) Based on the physical test, it was demonstrated that the precipitation-induced landslide in fully weathered granite initiated with a precipitation intensity of 155 mm/d, and the landslide occurred with an accumulated precipitation of 304 mm. Since this test used a laboratory-made slope, the original weathered rock mass structure was destroyed, thus the slopes of physical model and prototype were different. However, the results indicated the following sequence of events: precipitation infiltration → slope response → slope failures, which can be used to understand the internal mechanism of precipitation-induced landslides.

Declarations

Acknowledgements

This work was supported by the Hubei Provincial Natural Science Foundation (Grant No. 2016CFA023) and China Geological Survey Project Foundation (Grant No. DD20160257 & DD20190304).

References

Bai S, Wang J, Thiebes B, et al. (2014) Analysis of the relationship of landslide occurrence with rainfall: A case study of Wudu County, China. Arabian Journal of Geosciences 7(4): 1277-1285.

Chen H, Lee C F. (2003) A dynamic model for rainfall-induced landslides on natural slopes. Geomorphology 51(4): 269-288.

Dai FC, Lee CF. (2001) Frequency–volume relation and prediction of rainfall-induced landslides. Engineering Geology 59(3-4): 253-266.

Dietrich W E, Reiss R, Hsu M L, et al. (1995) A process-based model for colluvial soil depth and shallow landsliding using digital elevation data. Hydrological Processes 9(3/4): 383-400.

Heller V. (2011) Scale effects in physical hydraulic engineering models. Journal of Hydraulic Research 49(3): 293-306.

Huang R, Fan X. (2013) The landslide story. Nature Geoscience 6(5): 325-326.

Li C, Ma T, Zhu X, et al. (2011) The power–law relationship between landslide occurrence and rainfall level. Geomorphology 130(3-4): 221-229.

Li Y, Meng H, Dong Y, et al. (2004) Main types and characteristics of geo-hazard in China-Based on the results of geo-hazard survey in 290 counties. The Chinese Journal of Geological Hazard and Control 15(2): 29-31. (in Chinese)

Liu G, Li C, Lu B, et al. (2020) Model test of shallow failure of fully strong weathered rock slope induced by rainfall. Journal of Yangtze River Scientific Research Institute 37(7): 88-95.

Liu Y, Huang R, Huo J. (2008) Study on stability evaluation and protection measures of weathered granite slope in a certain expressway. Journal of Disaster Prevention and Mitigation Engineering 28(1): 19-25.

Pradhan A M S, Kim Y T. (2014) Relative effect method of landslide susceptibility zonation in weathered granite soil: a case study in Deokjeok-ri Creek, South Korea. Natural Hazards 72(2): 1189-1217.

Pradhan A M S, Kim Y T. (2015) Application and comparison of shallow landslide susceptibility models in weathered granite soil under extreme rainfall events. Environmental Earth Sciences 73(9): 5761-5771.

Segoni S, Piciullo L, Gariano SL. (2018) A review of the recent literature on rainfall thresholds for landslide occurrence. Landslides 15(8): 1483-1501.

Zêzere J L, Vaz T, Pereira S, et al. (2015) Rainfall thresholds for landslide activity in Portugal: a state of the art. Environmental Earth Sciences 73(6): 2917-2936.

Zheng M, Jian W, Wu M. (2005) Reliability analysis of stability of granite residual soil slope. Chinese Journal of Rock Mechanics and Engineering 24(2): 5337-5340. (in Chinese)

Figures

Figure 1

Typical fully weathered granite landslide in Fengkai County

Figure 2

Physical experiment model

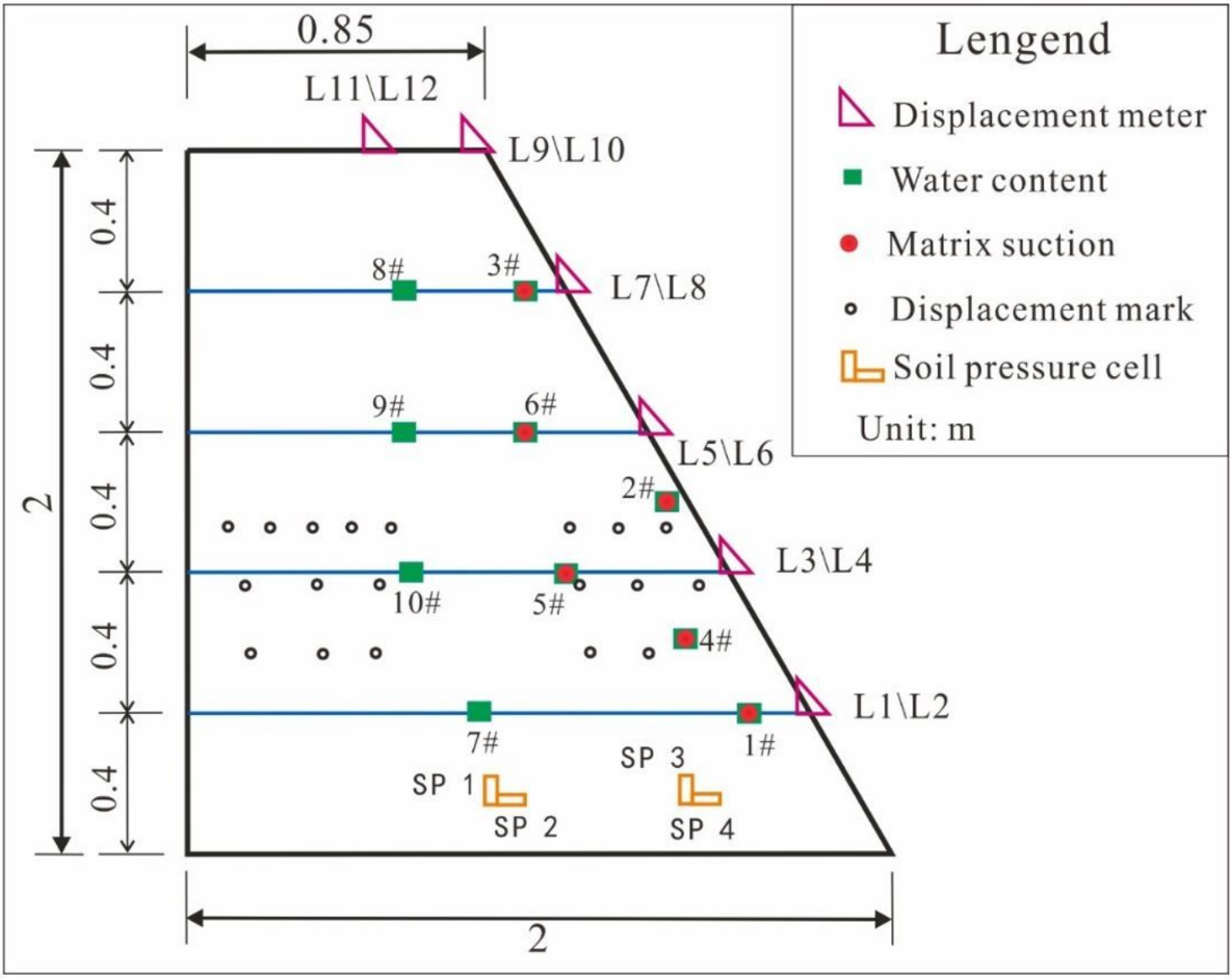

Figure 3

Physical model experiment scheme

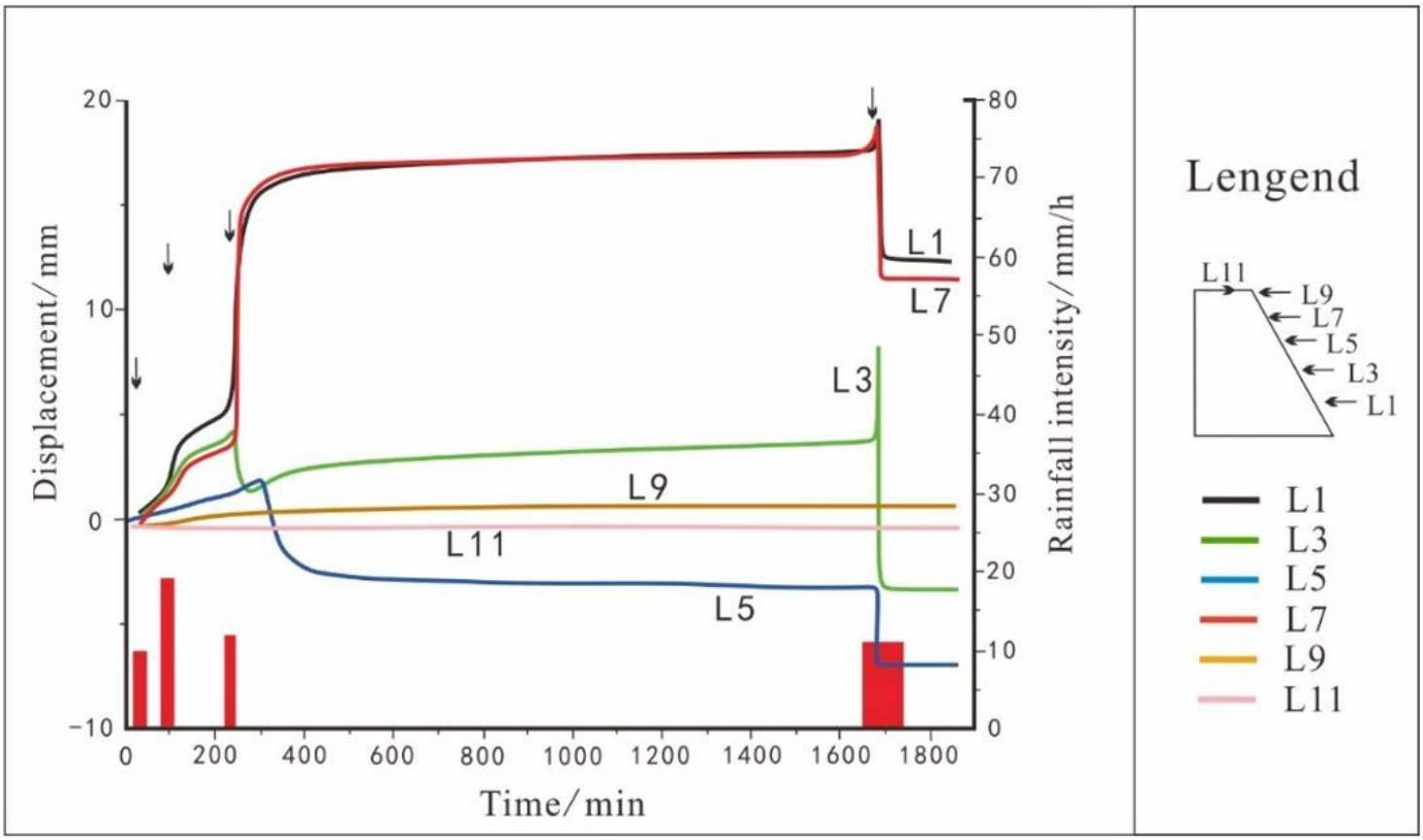

Figure 4

Slope horizontal deformation response curve under precipitation infiltration

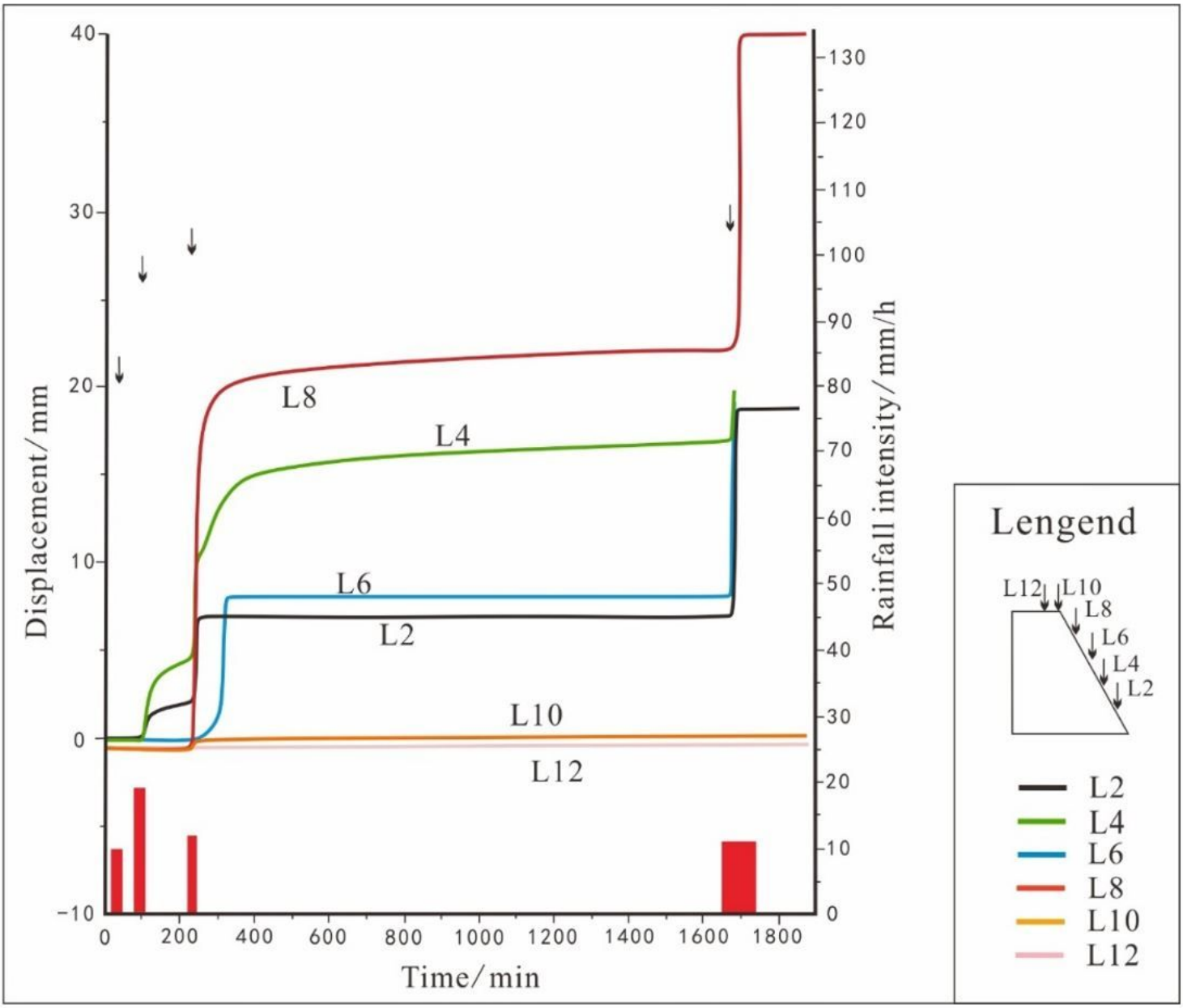

Figure 5

Slope vertical deformation response curve under precipitation infiltration

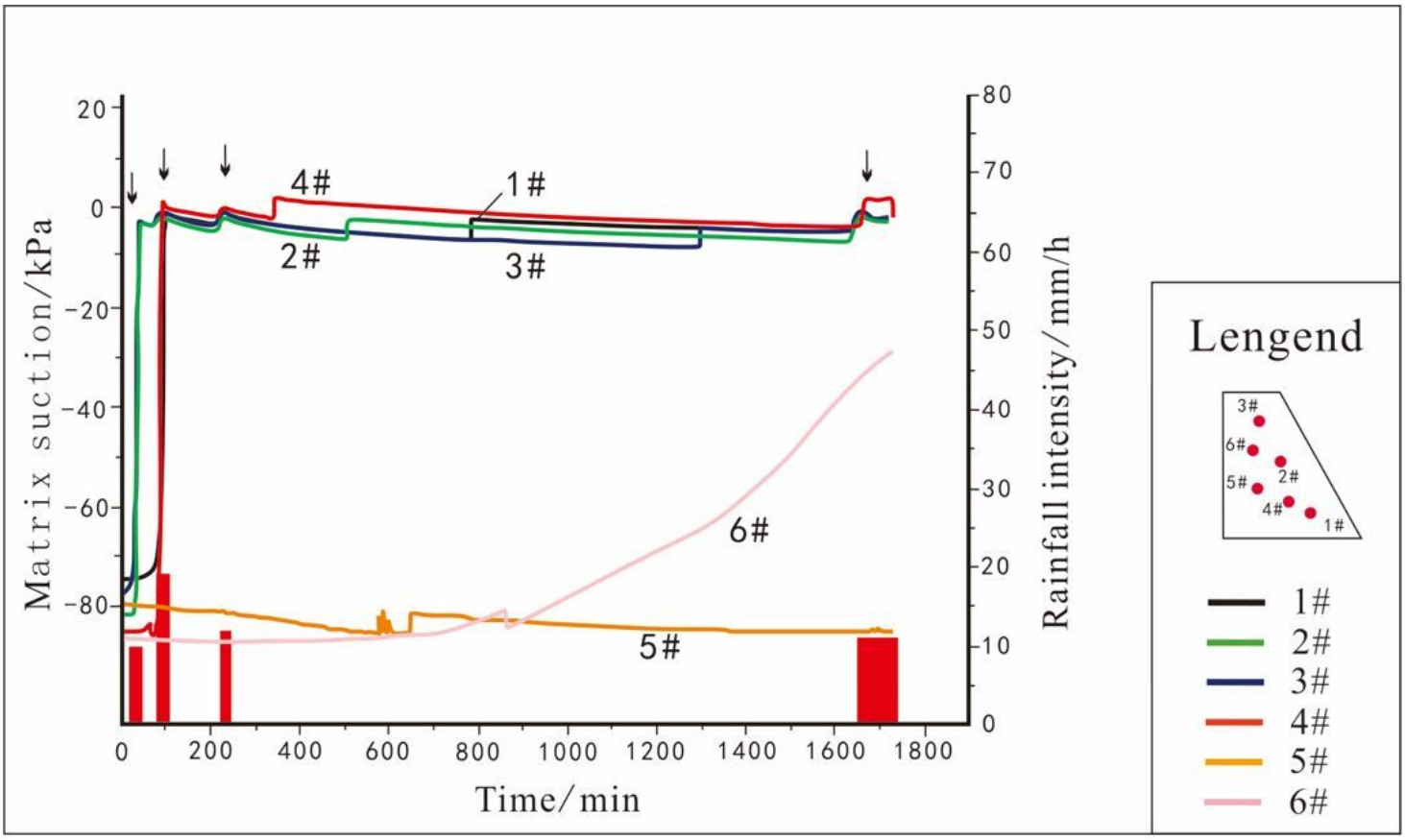

Figure 6

Slope matrix suction response curve under precipitation infiltration

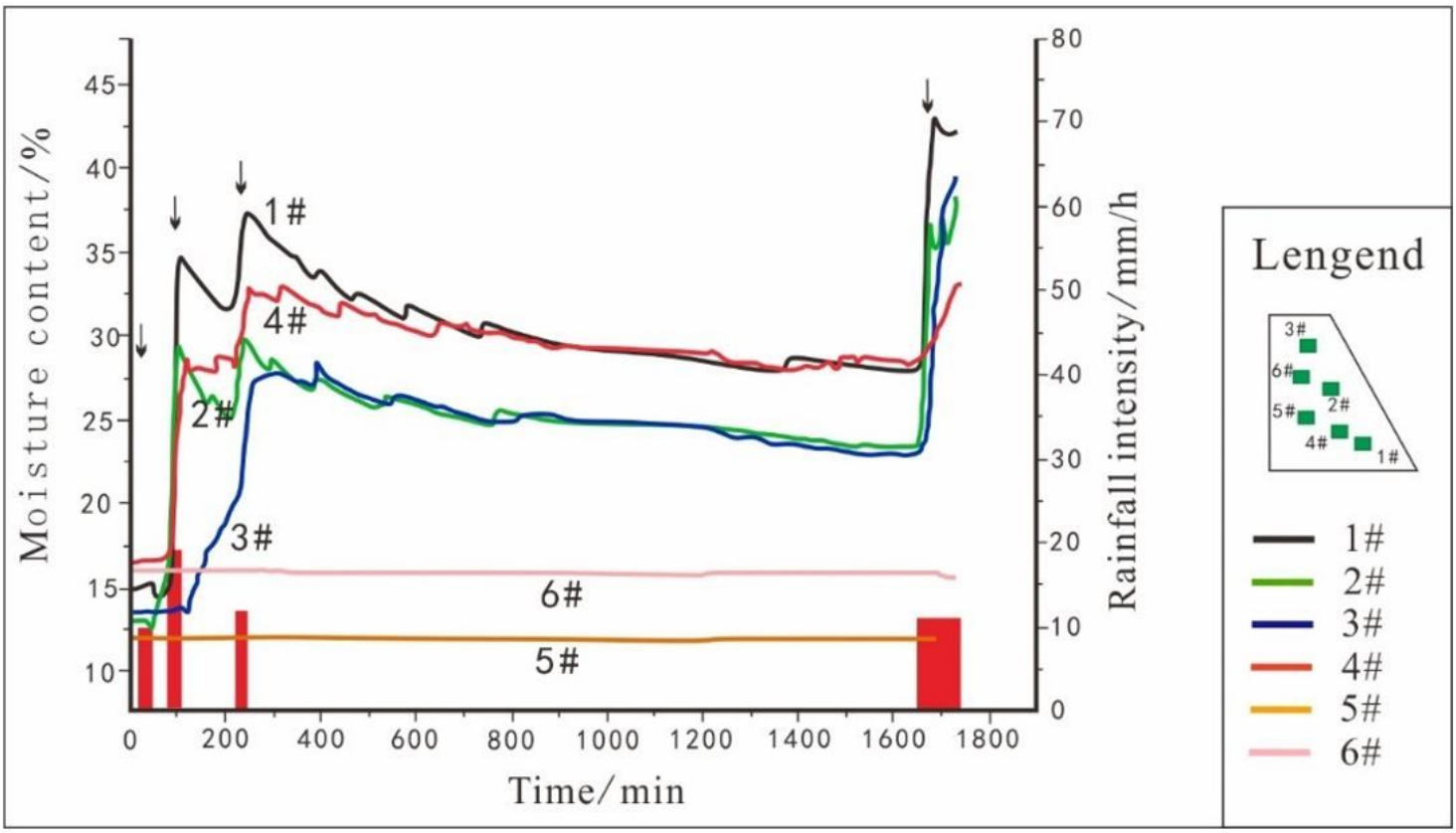

Figure 7

Slope moisture content response curve of precipitation infiltration

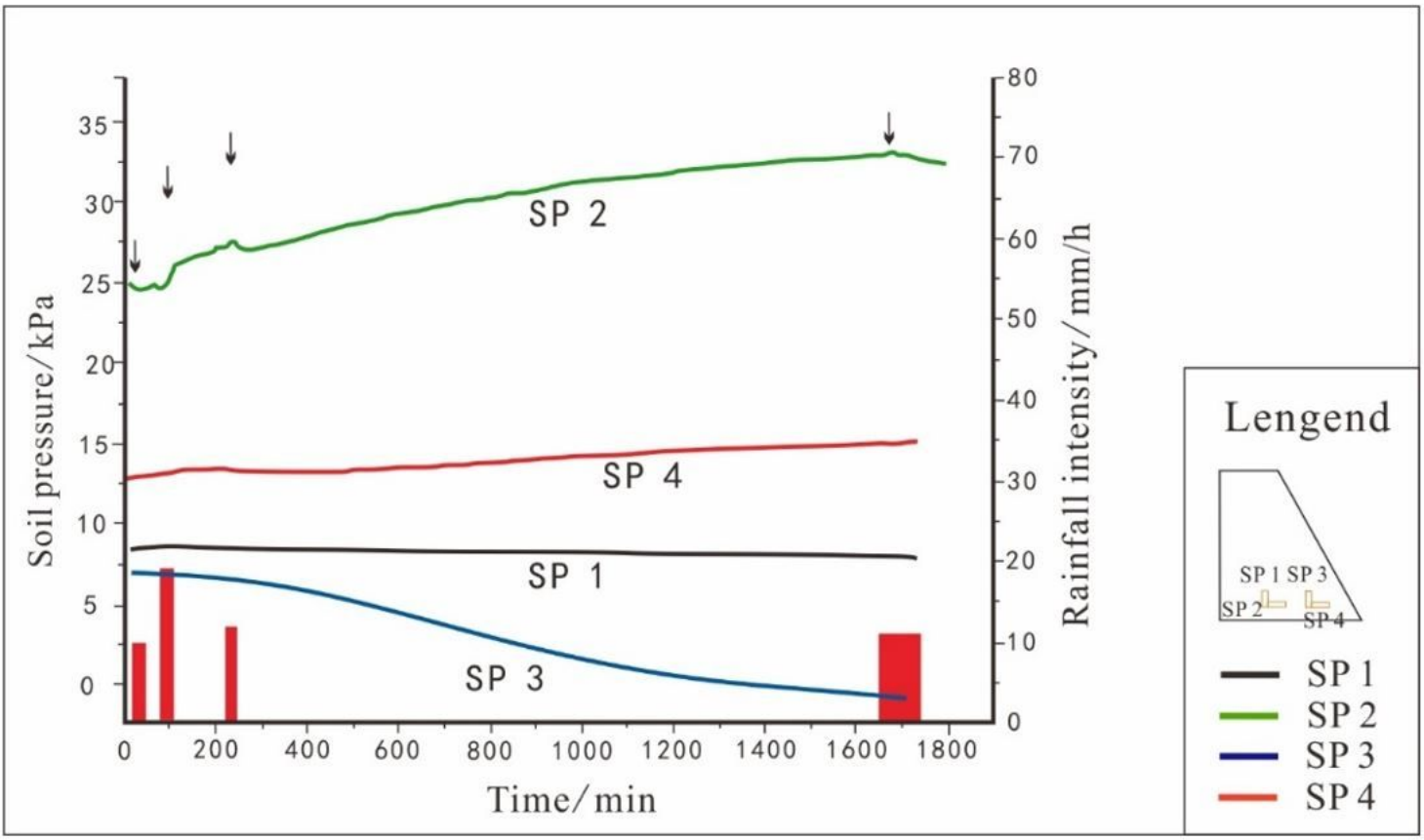

Figure 8

Soil pressure response curve of under precipitation infiltration

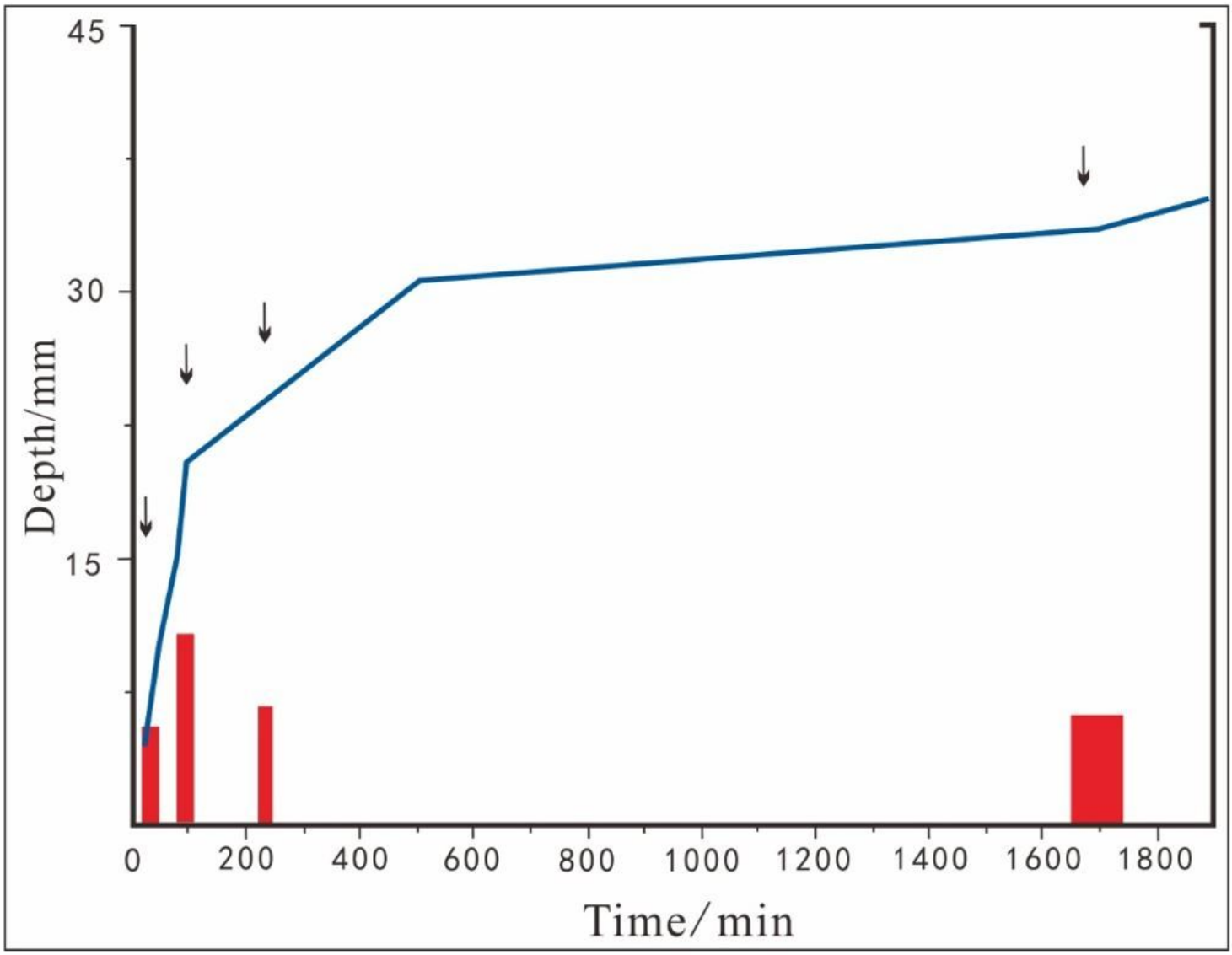

Figure 9

Response curve of slope wetting peak under precipitation infiltration

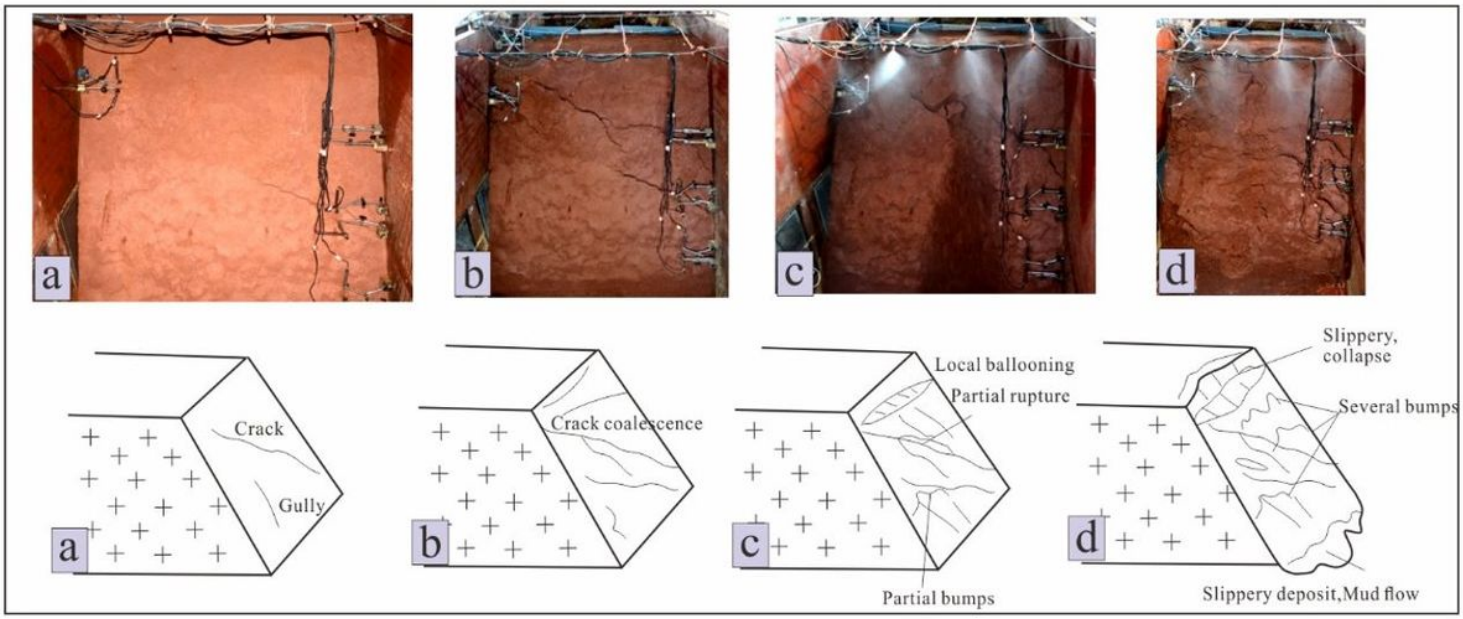

Figure 10

Failure process of fully weathered granite slope